Li *et al. Satellite Navigation* (2022) 3:20
https://doi.org/10.1186/s43020-022-00081-3

Satellite Navigation
https://satellite-navigation.springeropen.com/

ORIGINAL ARTICLE Open Access

Multi-GNSS products and services at iGMAS Wuhan Innovation Application Center: strategy and evaluation

Xingxing Li*, Qingyun Wang, Jiaqi Wu, Yongqiang Yuan, Yun Xiong, Xuewen Gong and Zhilu Wu

Abstract

Over the past years the International Global Navigation Satellite System (GNSS) Monitoring and Assessment System (iGMAS) Wuhan Innovation Application Center (IAC) dedicated to exploring the potential of multi-GNSS signals and providing a set of products and services. This contribution summarizes the strategies, achievements, and innovations of multi-GNSS orbit/clock/bias determination in iGMAS Wuhan IAC. Both the precise products and Real-Time Services (RTS) are evaluated and discussed. The precise orbit and clock products have comparable accuracy with the precise products of the International GNSS Service (IGS) and iGMAS. The multi-frequency code and phase bias products for Global Positioning System (GPS), BeiDou Navigation Satellite System (BDS), Galileo navigation satellite system (Galileo), and GLObal NAvigation Satellite System (GLONASS) are provided to support multi-GNSS and multi-frequency Precise Point Positioning (PPP) Ambiguity Resolution (AR). Compared with dual-frequency PPP AR, the time to first fix of triple-frequency solution is improved by 30%. For RTS, the proposed orbit prediction strategy improves the three dimensional accuracy of predicted orbit by 1 cm. The multi-thread strategy and high-performance matrix library are employed to accelerate the real-time orbit and clock determination. The results with respect to the IGS precise products show the high accuracy of RTS orbits and clocks, 4–9 cm and 0.1–0.2 ns, respectively. Using real-time satellite corrections, real-time PPP solutions achieve satisfactory performance with horizontal and vertical positioning errors within 2 and 4 cm, respectively, and convergence time of 16.97 min.

Keywords: iGMAS Wuhan Innovation Application Center, GREAT software, Precise orbit determination, Precise clock estimation, Observation-specific bias, Precise point positioning, Real-time service

Introduction

With the completion of BeiDou-3 Navigation Satellite System (BDS-3) (BDS-3, Yang et al., 2020) and Galileo navigation satellite system (Galileo), and the modernization of Global Positioning System (GPS) and GLObal NAvigation Satellite System (GLONASS) (Li et al., 2014), Global Navigation Satellite System (GNSS) has entered the era of multi-frequency and multi-constellation. The rapid development of GNSS brings new opportunities for high-precision navigation and positioning. However, the compatibility and interoperability among GNSS systems and signals have also become new challenges (Banville et al., 2020).

Stable and reliable multi-GNSS products are essential to fully exploit the potential of satellite resources. In mid-2011, the International GNSS Service (IGS, Dow et al., 2009) initiated the Multi-GNSS Experiment (MGEX, Montenbruck et al., 2017) to collect multi-GNSS data and provide various products. Soon after, China started the International GNSS Monitoring and Assessment System (iGMAS, Chen et al., 2015), which commits to monitor and evaluate the status of GNSS constellations and provide precise products.

*Correspondence: xxli@sgg.whu.edu.cn

School of Geodesy and Geomatics, Wuhan University, 129 Luoyu Road, Wuhan 430079, China

Nowadays, iGMAS and several IGS/MGEX Analysis Centers (ACs), like the Centre National d'Etudes Spatiales and Collecte Localisation Satellites (CNES/CLS, Loyer et al., 2012), Center for Orbit Determination in Europe (CODE, Dach et al., 2015), European Space Agency (ESA, Springer et al., 2017), GeoForschungsZentrum (GFZ, Uhlemann et al., 2014), Japan Aerospace Exploration Agency (JAXA), Shanghai Observatory (SHAO, Chen et al., 2012), Wuhan University (WHU, Guo et al., 2016), provide precise products publicly. Some of them, as well as Bundesamt für Kartographie und Geodäsie (BKG), Chinese Academy of Sciences (CAS), Deutsche Forschungsanstalt für Luftund Raumfahrt (DLR), GMV Aerospace and Defense (GMV), Natural Resources Canada (NRCan), also support RTS (Elsobeiey & Al-Harbi, 2016). However, GNSS users still suffer from occasional absence and long delay of products, and no any institutions provide a complete set of multi-frequency and/or multi-system products publicly. These problems are matters of concern yet, and will hinder the application and development of GNSS.

In order to support the development of domestic GNSS and alleviate the above-mentioned problems, iGMAS and WHU established the iGMAS Wuhan Innovation Application Center (iGMAS Wuhan IAC). A set of software named the GNSS + REsearch, Application and Teaching (GREAT, Li et al., 2021) was developed as a technical support. The Uncalibrated Phase Delay (UPD) estimation module of GREAT is in https://geodesy.noaa.gov/gps-toolbox. Currently, a suite of post-processed and real-time products covering as many constellations and frequencies as possible generated by the GREAT software is available. The former includes precise orbit, clock, and bias products needed for high-precision researches, while the latter refers to real-time satellite corrections, effectively supporting real-time applications.

In this contribution, the achievements and innovations of multi-GNSS products and Real-Time Services (RTS) are introduced, and the post-processed/real-time products are evaluated. The article is organized as follows. After the introduction, an overview of the GREAT software, products, and services is given in "Overview of multi-GNSS products and services" section. IGS/MGEX/iGMAS multi-GNSS products are summarized in "Precise multi-GNSS and multi-frequency products" section. Subsequently, the strategies applied in Precise Orbit Determination (POD), Precise Clock Estimation (PCE), and bias estimation are introduced with a focus on the IAC bias products. In "Assessment of precise GNSS products" section, the orbit, clock, and bias products are evaluated through multiple methods including Precise Point Positioning (PPP). Aside from presenting the status of RTS, "Real-time service" section introduces the strategies of ultra-rapid orbit determination and real-time clock estimation with an emphasis on the innovations of IAC. Then, "Assessment of real-time services" section assesses the accuracy of real-time products and real-time PPP (RTPPP) performance. Finally, the conclusions are summarized in "Conclusions" section.

Overview of multi-GNSS products and services

Starting a trial operation in Jun. 2020, iGMAS Wuhan IAC has been continuously providing precise GNSS products and services for more than two years, which are available for registered users at http://igmas.users.sgg.whu.edu.cn/products/download/. By Feb. 2022 total downloads exceeded 23,000 times.

As a powerful technical support, the GREAT software is widely used in the product generation of IAC. The GREAT software can satisfy the various demands of geodesy and navigation applications including post/real-time POD and PCE, multi-GNSS bias estimation, PPP Ambiguity Resolution (PPP-AR), PPP Real-Time Kinematic (PPP-RTK) with regional augmentation, Low-Earth-Orbit (LEO) augmented GNSS, and multi-sensor navigation. Written in standard C++11 language and compiled with Object-Oriented principle, the software is friendly to developers. In addition, the GREAT software supports most mainstream operating systems, such as Windows, Linux, and MacOS.

Figure 1 presents an overview of the multi-GNSS products and RTS of IAC. For high-precision GNSS applications, precise orbit and clock are generated in a routine mode with a latency of less than 40 h. Precise orbits at 300 s interval are determined first, and then 30 s interval clock are estimated with the orbits. Based on the orbit and clock products, signal biases originated in code and phase measurements of different systems and frequencies, e.g., code Observation-Specific Bias (OSB), phase OSB and Inter-Frequency Clock Bias (IFCB), can be precisely estimated. Except for post-processed products, RTS is provided to support real-time applications. The quad-system ultra-rapid orbits are released every 2 h, and real-time satellite corrections are broadcasted with the IGS State Space Representation (https://igs.org/rts/formats/) format using the Ntrip protocol.

Precise multi-GNSS and multi-frequency products

Precise products status

With the development of multi-GNSS, GNSS positioning accuracy is expected to be further improved. Among various GNSS products, high-quality orbit and clock products are the core for high-precision GNSS service (Steigenberger & Montenbruck, 2019). Table 1 presents an overview of multi-GNSS orbit/clock products for IGS/MGEX ACs, iGMAS, and IAC. Currently, CODE, ESA, GFZ, and WHU provide orbit/clock products for five

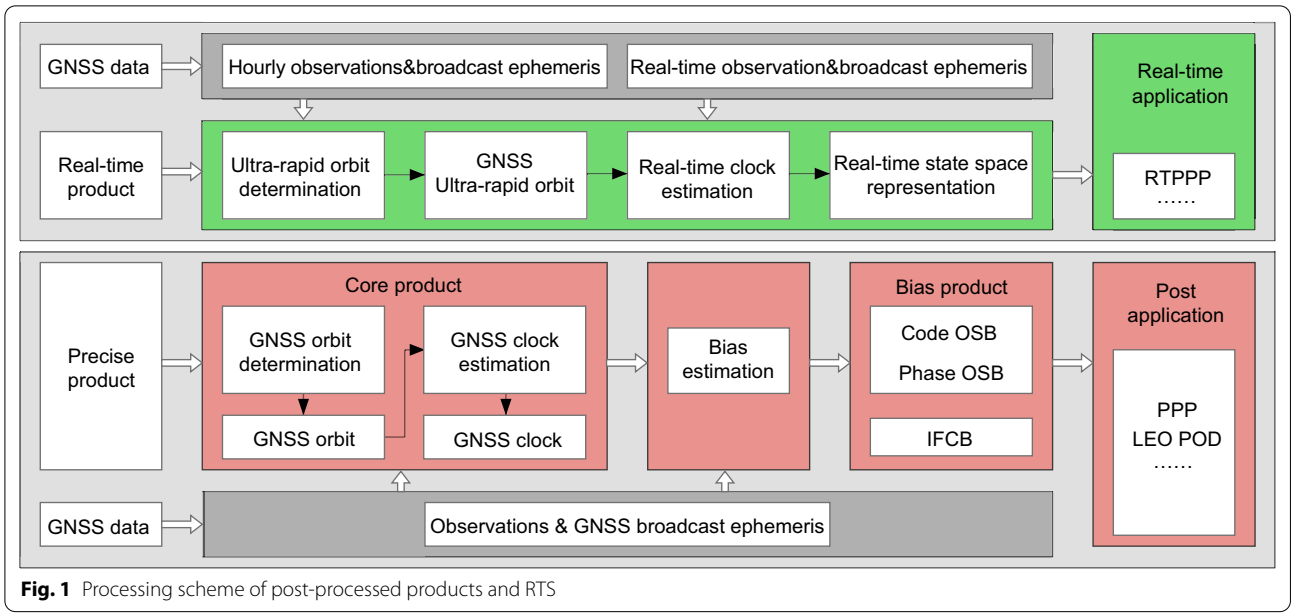

Fig. 1 Processing scheme of post-processed products and RTS

Table 1 Overview of precise orbit/clock products as of January 2022

Institution name	System	Interval (orbit/clock)	Remarks	References
CODE	G, C, E, R, J	5 min/30 s	BDS GEOs excluded; J07 excluded	Prange et al. (2017)
ESA	G, C, E, R, J	5 min/30 s	BDS GEOs excluded; J07 excluded	Mayer et al. (2018)
GFZ	G, C, E, R, J	5 min/30 s		Uhlemann et al. (2014)
WHU	G, C, E, R, J	15 min/30 s		Guo et al. (2016)
SHAO	G, C, E, R	5 min/5 min		Chen et al. (2014)
CNES/CLS	G, E, R	5 min/30 s		Loyer et al. (2016)
JAXA	G, R, J	5 min/30 s		
iGMAS	G, C, E, R	15 min/5 min	Combined solutions	Zhou et al. (2022)
IAC	G, C, E, R	5 min/30 s	BDS GEOs excluded	

systems, GPS, BDS, Galileo, GLONASS, and Japanese Quasi-Zenith Satellite System (QZSS). The quad-system orbit/clock products including GPS, BDS, Galileo, and GLONASS are available at SHAO, iGMAS, and IAC. Note that BDS Geostationary Earth Orbit (GEO) satellites are not considered in CODE, ESA, and IAC due to their long revolution time (1 d), poor observability, and frequent satellite maneuvers (Prange et al., 2017). Specifically, "COD", "ESM", "GBM", "WUM", "SHA", "GRG", "JAX", and "ISC" are used to denote multi-GNSS products from CODE, ESA, GFZ, WHU, SHAO, CNES/CLS, JAXA and iGMAS, respectively. The products of IAC are referred as "GRT" generated with GREAT software. In the table, letters G, C, E, R, and J denote GPS, BDS, Galileo, GLONASS, and QZSS, respectively.

To fully use satellite and signal resources, the signal biases originating from different systems and different frequencies must be precisely modeled and corrected. Table 2 gives an overview of bias products from domestic and international institutions. The P1C1, P1P2, and P1P2 Differential Code Bias (DCB) products generated by CODE have been widely used in the GNSS community. However, the legacy DCB product is monthly updated, and only contains the bias data of GPS and GLONASS. Due to the soaring number of possible combined forms in multi-frequency data processing (Villiger et al., 2019), traditional differential signal bias products show less flexibility and convenience. Recently, daily-updated bias products for multi-GNSS and multi-frequency signals have been released by institutions like CAS, CNES/CLS, CODE, DLR, and WHU. Nevertheless, the current bias products still have some problem. GLONASS phase bias remains absent, and only dual-frequency phase biases are provided for GPS, BDS, and Galileo. Moreover, although

Table 2 Overview of bias products as of January 2022

Bias product	Institution name	System	Number of frequency	References
DCB	CODE	G, R	2, 2	https://www.aiub.unibe.ch/research
	CAS	G, C, E, R, J	3, 6, 5, 2, 3	Wang et al. (2016)
	DLR	G, C, E, R, J	3, 6, 5, 2, 3	Montenbruck et al. (2014)
	iGMAS	G, C, E, R	2, 2, 2, 2	www.igmas.org
Code OSB	CODE	G, C, E, R, J	2, 2, 2, 2, 2	
	WHU	G, C, E, R, J	3, 6, 5, 2, 3	
	CAS	G, C, E, R	3, 6, 5, 2	
	CNES/CLS	G, E	2, 2	
	IAC	G, C, E, R	3, 6, 5, 2	
Phase OSB	WHU	G, C, E	2, 2, 2	Geng et al. (2019)
	CODE	G, E	2, 2	Schaer et al. (2021)
	CNES/CLS	G, E	2, 2	Rovira-Garcia et al. (2021)
	IAC	G, C, E, R	3, 4, 3, 2	

many researches have proved the indispensability of IFCB in multi-frequency GNSS positioning (Montenbruck et al., 2012; Zhao et al., 2019), public IFCB products are still unavailable.

Precise orbit and clock determination

IAC POD and PCE adopt the similar strategies as the IGS rapid product (see Table 3). More than 150 MGEX stations with stable and high-quality observations are used in a routine process (POD, PCE and bias estimation). Note that GLONASS observations contain the Inter-Frequency Bias (IFB), which is receiver-type specific and cannot be appropriately modeled (Wanninger et al., 2007). Coupling with the phase ambiguity parameter, the GLONASS IFB discourages the phase bias estimation and AR. Therefore, the ambiguities of GLONASS observations are not fixed in POD. According to the classification of station receiver types, it is feasible to avoid this problem by estimating the phase biases for the stations with the same receiver type every time.

Table 3 Processing strategies for POD and PCE

Item	Model
Observations	Undifferenced code and phase Ionospheric-Free (IF) combination observations
Sampling rate	300 s (POD); 30 s (PCE)
Arc length	1 d
Elevation cutoff	7°
Weighting	Elevation-dependent weighting with priori accuracy of 0.003 cycles and 0.3 m for raw phase and code observations
Satellite antenna	igs14.atx (Rebischung et al., 2016)
Receiver antenna	igs14.atx
Ionospheric delay	IF combination eliminated 1st order effect; higher order not considered
Tropospheric delay	Global Mapping Function (GMF); Saastamoinen model for dry hydrostatic delay; wet part estimated as piecewise constants
Tide forces	Solid Earth tide, pole tide, ocean tide loading
Relativistic effect	International Earth Rotation and Reference Systems Service (IERS) Conventions 2010 (Petit & Luzum, 2010)
Phase wind-up	Correct (Wu et al., 1993)
Geopotential	Earth Gravitational Model (EGM), 12 × 12 (Nikolaos et al., 2012)
N-body gravitation	Sun, Moon and other planets; Jet Propulsion Laboratory (JPL) DE421 (Folkner et al., 2009)
Solar radiation pressure (SRP) model	5-parameter ECOM (Extend CODE Orbit Model, Arnold et al., 2015) for GPS/BDS/GLONASS; ECOM2 (D0, D2c, D2s, D4c, D4s, Y0, X0, X1c, X1s) (Prange et al., 2017) for Galileo
Estimator	The least squares
Station coordinates	Fixed to IGS weekly solutions
Ambiguities	Estimated as constant value for a continuous arc
Earth rotation	Estimate XPOLE, YPOLE, DXPOLE, DYPOLE, UT1, DUT

Code and phase bias estimation

Methods

The Geometry-Free and Ionospheric-Free (GFIF) combination can eliminate frequency-independent components, and is useful for IFCB estimation (Li et al., 2012; Montenbruck et al., 2012). GFIF combination of phase observation L can be expressed as:

$$L_{\mathrm{GFIF}} = L_{\mathrm{IF}(m,n)} - L_{\mathrm{IF}(m,k)} = \delta + b_{r,\mathrm{GFIF}} - b^{s}_{\mathrm{GFIF}} \quad (1)$$

where the superscripts s and subscript r indicate satellite and receiver, respectively; m, n and k denote the frequency; GFIF is a linear combination of m, n and k; IF is the Ionosphere-Free combination; N is the carrier phase ambiguity in meter; b is the phase hardware delay in meter; δ is the phase IFCB (PIFCB).

If there are no cycle slips between adjacent epochs, the changes of N and b between epochs are small enough to be ignored. Therefore, the Epoch-Differenced (ED) phase IFCB can be obtained by the ED GFIF combination:

$$\Delta\delta(t, t-1) = L_{\mathrm{GFIF}}(t) - L_{\mathrm{GFIF}}(t-1) \quad (2)$$

Then, each epoch PIFCB values can be recovered by a cumulative method:

$$\delta(t) = \delta(t_0) + \sum_{j=0}^{t-1} \Delta\delta(j, j+1) \quad (3)$$

where $\delta(t)$ refers to the undifferenced PIFCB value at epoch t; t_0 refers to the reference epoch. Usually, there are generally two methods to determine PIFCB at the reference epoch: one is set to 0, and the other is the zero-mean constraint over the whole estimated period. The GREAT software employs the latter.

The UPD can be estimated by the least square adjustment with derived float ambiguities. The float N can be split into the sum of integer ambiguity $\overline{N}$ and UPD b at receiver and satellite sides:

$$N = \overline{N} + b_r - b^{s} \quad (4)$$

Then, the UPD is estimated first for wide-lane (WL) and extra-wide-lane (EWL) and then for narrow-lane (NL). The Hatch–Melbourne–Wübbena (HMW) combination of pseudorange observation P and phase observation L (Hatch, 1983; Melbourne, 1985; Wübbena, 1985) is formed to calculate WL and EWL ambiguities:

$$\begin{aligned} N_{\mathrm{WL}} &= \frac{L_m}{\lambda_m} - \frac{L_n}{\lambda_n} - \frac{f_m P_m + f_n P_n}{(f_m + f_n)\lambda_{\mathrm{WL}}} \\ N_{\mathrm{EWL}} &= \frac{L_n}{\lambda_n} - \frac{L_k}{\lambda_k} - \frac{(1-\alpha)P_m + \alpha P_n}{\lambda_{\mathrm{EWL}}} \end{aligned} \quad (5)$$

with:

$$\alpha = \frac{f_m^2 f_n + f_n^2 f_k}{f_k\left(f_m^2 - f_n^2\right)} \quad (6)$$

where f is the frequency of corresponding code measurement; λ is the wavelength of carrier phase measurement.

Hereafter, the NL ambiguity can be derived from the combination of estimated IF ambiguity and integer WL ambiguity, which is formulated as:

$$N_{\mathrm{NL}} = \frac{f_m + f_n}{c} N_{\mathrm{IF}(m,n)} - \frac{f_n}{f_m - f_n}\overline{N}_{\mathrm{WL}} \quad (7)$$

Then, receiver and satellite WL, EWL, and NL UPDs are estimated using least square adjustment. At last, the code OSB B and phase OSB $B^{'}$ on frequency m, n and k can be defined with DCB D and UPD b as:

$$\begin{cases} B^{s}_{m} = -\dfrac{f_n^2}{f_m^2 - f_n^2} D^{s}_{m,n} \\ B^{s}_{n} = -\dfrac{f_m^2}{f_m^2 - f_n^2} D^{s}_{m,n} \\ B^{s}_{k} = B^{s}_{m} - D^{s}_{m,k} \end{cases} \quad (8)$$

$$\begin{cases} B^{'}_{m} = \dfrac{\lambda_m b^{s}_{\mathrm{WL}}}{\lambda_m - \lambda_n} - \dfrac{\lambda_n B^{s}_{m} + \lambda_m B^{s}_{n}}{\lambda_n(\lambda_m + \lambda_n)} + b^{s}_{\mathrm{NL}} \cdot \dfrac{(\lambda_m + \lambda_n)\cdot c}{\lambda_m \lambda_n (f_m + f_n)} \\ B^{'}_{n} = \dfrac{\lambda_n b^{s}_{\mathrm{WL}}}{\lambda_m - \lambda_n} + \dfrac{\lambda_n B^{s}_{m} + \lambda_m B^{s}_{n}}{\lambda_m(\lambda_m + \lambda_n)} + b^{s}_{\mathrm{NL}} \cdot \dfrac{(\lambda_m + \lambda_n)\cdot c}{\lambda_m \lambda_n (f_m + f_n)} \\ B^{'}_{k} = \dfrac{\lambda_n - \lambda_k}{\lambda_n + \lambda_k}\left(\dfrac{B^{s}_{n}}{\lambda_n} + \dfrac{B^{s}_{k}}{\lambda_k}\right) + B^{'}_{n} - b^{s}_{\mathrm{EWL}} \end{cases} \quad (9)$$

Strategy

Based on the method in "Methods" section, IAC generates OSB and IFCB products by fully exploting the multi-frequency signals of GPS, BDS, Galileo, and GLONASS. Then, PPP users can achieve multi-GNSS and multi-frequency AR easily. Table 4 lists the GNSS signals involved in the bias estimation, and the reference signals of each system are marked by '√'.

Figure 2 exhibits the procedure of OSB and IFCB estimations. Firstly, raw code observations and ionosphere corrections are adopted for extracting DCB. The satellite-included code biases in BDS code observations are corrected with an elevation-dependent empirical model (Wanninger & Beer, 2015). Meanwhile, IFCB is acquired by the ED approach based on GFIF combination. Based on DCB and IFCB, WL and EWL ambiguities can be derived from the HMW combination, while NL

Table 4 GNSS signals in phase and code OSB estimation

System	GNSS signal	
	Phase observation	Code observation
GPS	L1	C1C; C1W (√)
	L2	C2L; C2W (√); C2X
	L5	C5Q; C5X
BDS	B1C	C1P; C1X
	B1I	C2I (√); C2X
	B2a	C5P; C5X
	B2I	C7I (√)
	B3I	C6I (√)
Galileo	E1	C1X (√)
	E5a	C5X (√)
	E5b	C7X
	E5ab	C8X
	E6	C6X
GLONASS	L1	C1C (√)
	L2	C2C (√)

ambiguities are calculated using precise orbit and clock. Afterwards, WL and NL UPDs are estimated with a least squares estimator. Finally, the absolute code and phase biases can be converted from differential format according to their linear relationship.

Assessment of precise GNSS products

This section evaluates the precise products. The orbit and clock products from DOY 001 to 300, 2021 are compared with the precise products from several institutions, and SLR observations are adopted for independent orbit assessment. For bias products, the stability in different time scales is assessed and demonstrated. Moreover, PPP AR is carried out to evaluate the overall performance of the precise orbit, clock, and bias products.

GNSS orbit products

Orbit comparison with precise products

The differences between GRT orbits and the final products of iGMAS and IGS/MGEX ACs at 300 s sampling

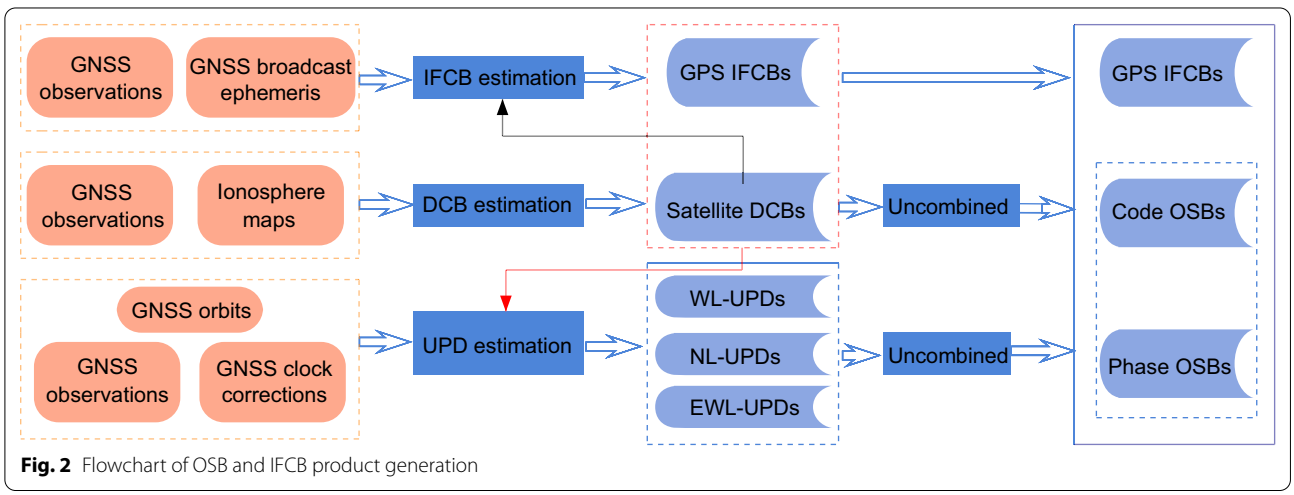

Fig. 2 Flowchart of OSB and IFCB product generation

Table 5 Comparison of processing strategies

Institution name	Software	Differencing	Elevation (°)	Arc length (d)	SRP model
CODE	Bernese	Orbit: DD[a] Clock: UD[b]	Orbit: 3 Clock: 5	3	ECOM2
GFZ	EPOS.P8	UD	7	3	ECOM
WHU	PANDA	UD	7	1	ECOM
SHAO	PANDA	UD	7	3	Unknown
IAC	GREAT	UD	7	1	Galileo: ECOM2 Other: ECOM

[a] DD stands for double differenced observation model

[b] UD stands for un-differenced observation model

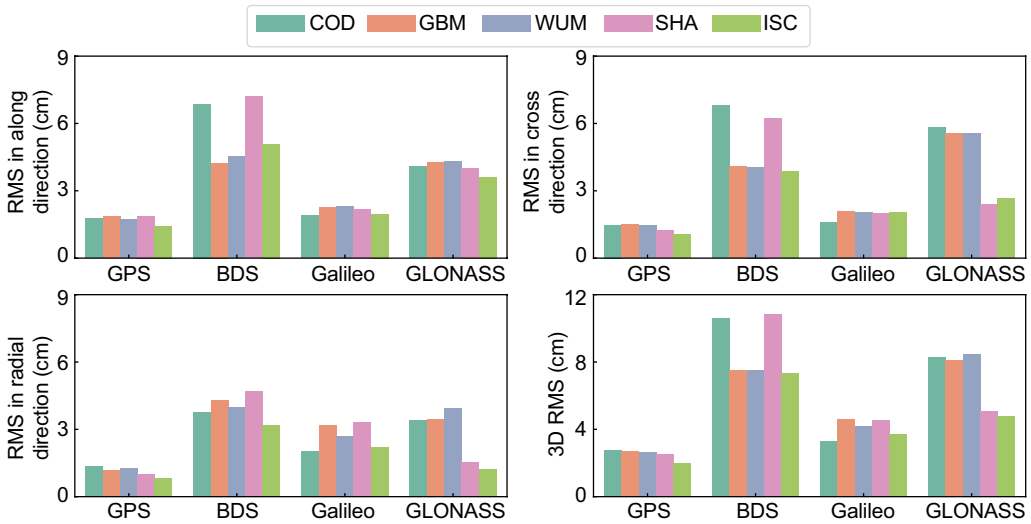

Fig. 3 Average RMSs of GRT GPS, BDS, Galileo, and GLONASS orbits in along-, cross-track, and radial directions compared with COD, GBM, WUM, SHA, and ISC orbits as reference

rate are calculated. Table 5 summaries the orbit/clock processing strategies of CODE, GFZ, WHU, and SHAO (Guo et al., 2017; Li et al., 2020), while iGMAS is the combined product of iGMAS ACs. The results are presented with Root Mean Square (RMS) values in along-, cross-track, and radial components in Fig. 3. Considering the inconsistency among the products of different institutions, a Helmert transformation is employed to eliminate systematic errors (Guo et al., 2016).

It can be seen from the figure that GPS orbits show the highest consistency, with an average Three-Dimension (3D) RMS of 2.11 cm, followed by Galileo 3.39 cm, GLONASS 5.79 cm and BDS 7.30 cm. The results of GPS and Galileo from the five institutions demonstrate little differences. However, orbit differences of BDS by CODE and SHAO are obviously larger in along- and cross-track directions. For GLONASS, the RMSs by CODE, GFZ, and WHU are significantly larger than those by SHAO and iGMAS. The larger differences can be attributed to the shorter arc length and different SRP models mentioned in Table 5. On the whole, GRT orbits show a good agreement with precise orbit products, and can meet the needs for precise GNSS applications.

SLR validation

Satellite Laser Ranging (SLR) provides an independent assessment of derived orbits because of its high-accuracy distance observation. For BDS and Galileo satellites equipped with laser retroreflector array, SLR validation results of GRT orbits are calculated, and compare with those of COD, WUM, and ISC orbits. Figure 4 displays the time series for GRT SLR residuals of 4 satellites belonging to BDS-2, BDS-3, Galileo In-Orbit Validation (IOV) and Galileo Full Operational Capability (FOC), respectively. Table 6 summarizes the mean bias and Standard Deviation (STD) of SLR residuals with the outliers greater than 0.4 m excluded.

For BDS-2 satellites, the STDs of GRT orbits are between 4.3 and 5.8 cm for Medium Earth Orbit (MEO) and Inclined Geosynchronous Orbit (IGSO) satellites. For BDS-3 satellites, the China Academy of Space Technology (CAST, C20 and C21) and Shanghai Engineering Center for Microsatellites (SECM, C29 and C30) satellites, there are opposite patterns of SLR residuals with the mean bias of 2.72 and − 3.68 cm. The results are consistent with previous studies (Zhao et al., 2022). The WUM SECM orbits achieve a near zero mean bias, which may be contributed to the prior SRP models applied. The dispersion degree of the SLR residuals for GRT BDS-3 orbits is about 3.2 cm, which is smaller than that of BDS-2. Compared with ISC orbits, the SLR residuals of Galileo show smaller mean bias of 0.5~1.0 cm, with STDs of around 2.3 cm.

GNSS clock products

Similarly, GRT clock products are evaluated at 30 s sampling rate. G01, C16, E01, and R06 are used as reference satellites for GPS, BDS, Galileo, and GLONASS, respectively. The comparison results with reference to ISC, COD, GBM and WUM final products are expressed as STDs, and shown in Fig. 5.

Among the four systems, GPS and Galileo clock products show superior quality, with average STDs of less

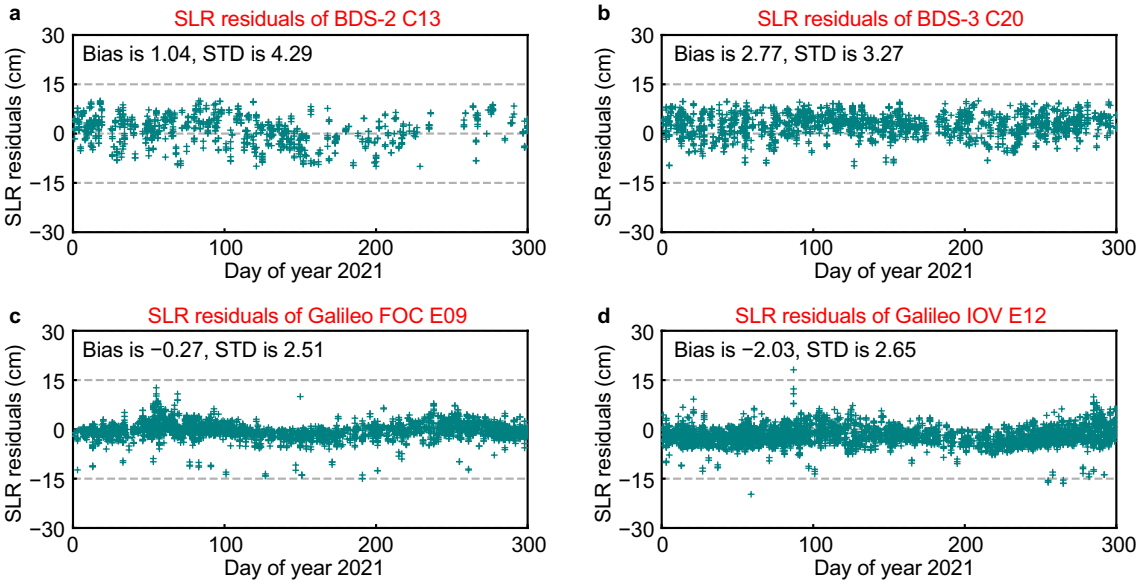

Fig. 4 SLR residuals of GRT C13, C20, E09, and E12 orbits

Table 6 SLR validation results of IAC, CODE, WHU, and iGMAS

Satellite type	Results of IAC (cm)		Results of CODE (cm)		Results of WHU (cm)		Results of iGMAS (cm)	
	Bias	STD	Bias	STD	Bias	STD	Bias	STD
BDS-2 IGSO	− 0.10	5.72	0.10	7.24	− 1.12	5.33	− 1.90	6.05
BDS-2 MEO	2.48	4.38	− 1.42	5.89	− 0.73	5.00	0.40	5.37
BDS-3 CAST MEO	2.72	3.18	4.30	2.77	3.67	3.15	1.72	3.32
BDS-3 SECM MEO	− 3.68	3.16	− 3.20	2.52	− 0.19	3.32	− 3.26	3.61
Galileo IOV	− 2.30	2.27	− 2.07	3.15	− 0.55	2.95	− 3.26	3.51
Galileo FOC	− 2.42	2.19	− 0.62	2.56	0.78	2.80	− 2.94	3.24

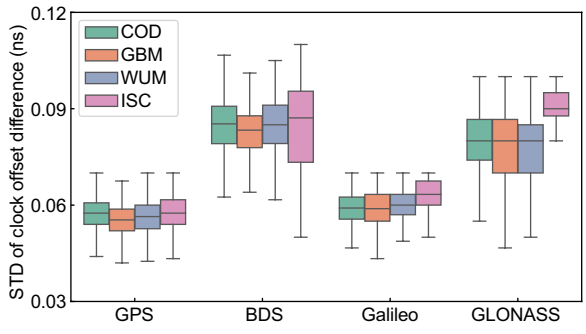

Fig. 5 STDs of GRT GPS, BDS, Galileo, and GLONASS clock compared with COD, GBM, WUM, and ISC clock products as reference

than 0.06 ns, followed by GLONASS and BDS about 0.08 ns. Moreover, the distribution of STDs is relatively concentrated, indicating the reliability of GRT clock products over a long period. On the whole, GRT clock products show a good consistency with GBM and WUM, followed by COD and ISC. The comparison results are basically consistent with orbit accuracy.

Bias products

Code and phase OSB evaluation

Stability is an important indicator of OSB products. Figure 6 depicts the 30 d code OSBs with two representative satellites per constellation, and Fig. 7 presents the

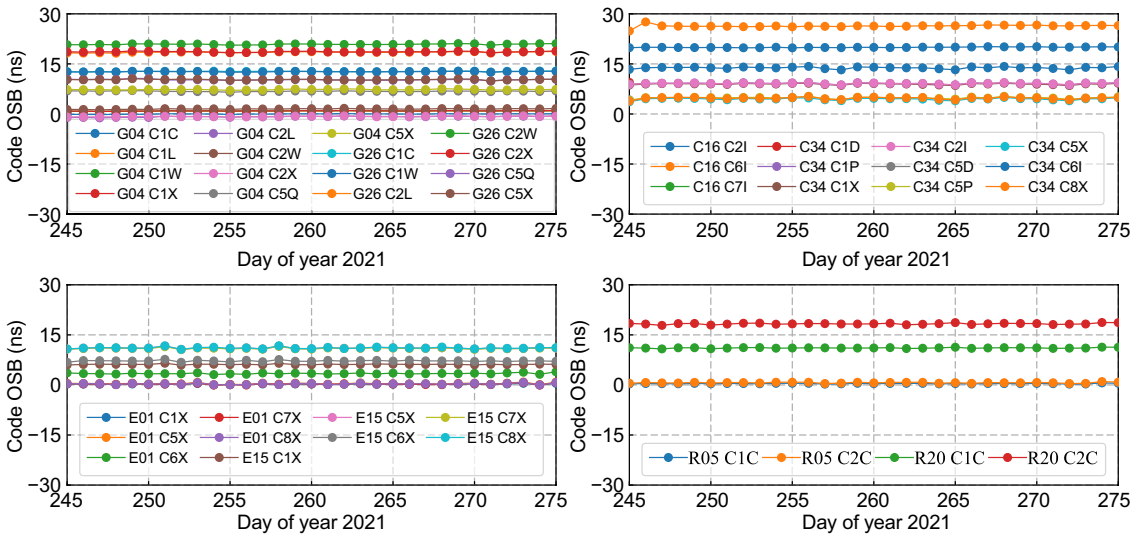

Fig. 6 Code OSBs for GPS, BDS, Galileo, and GLONASS on DOYs 246–275, 2021

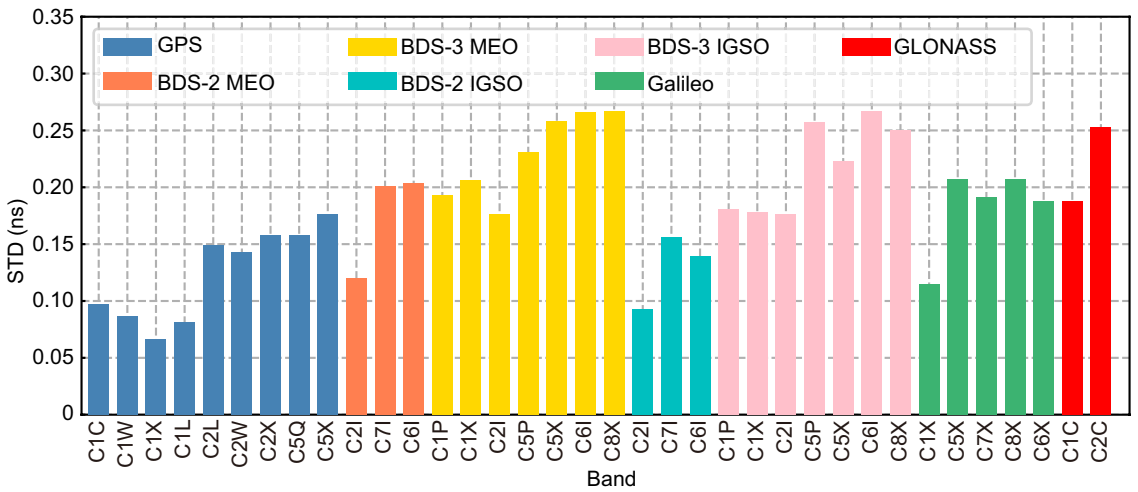

Fig. 7 Average STDs of the estimated code OSBs on DOYs 246–275, 2021

mean STDs. It can be seen that quad-system code biases can remain stable over long periods of time. For statistical analysis, the average STDs of all signals are less than 0.30 ns. Among them, STDs of GPS BLOCK III C1X and C1L (G04, G11, G14, G18, G23) signals are the smallest, indicating the excellent quality of BLOCK III L1C signal.

Figure 8 and Table 7 display the 24 h time series of phase OSBs and the average STD for each signal, respectively. For convenience, only the phase bias estimation results at the stations equipped with TRIMBLE receiver are shown in this contribution. As can be seen, the quad-system phase OSBs remain stable throughout the day. GPS and Galileo phase OSBs are comparably stable with an average STD of each signal less than 0.015 ns. The stability of BDS phase biases is slightly poor, and the STDs are all less than 0.045 ns. GLONASS phase biases show more fluctuations, and STDs of L1 and L2 are 0.074 and 0.096 ns, respectively. This may be caused by fewer GLONASS stations. Although the most GLONASS stations are equipped with TRIMBLE receiver, the number of available stations is around 80, which is significantly less than GPS/BDS/Galileo stations of around 200. Besides, some studies show new BDS-3 signals are comparable to GPS IIF and Galileo signals in terms of phase and code

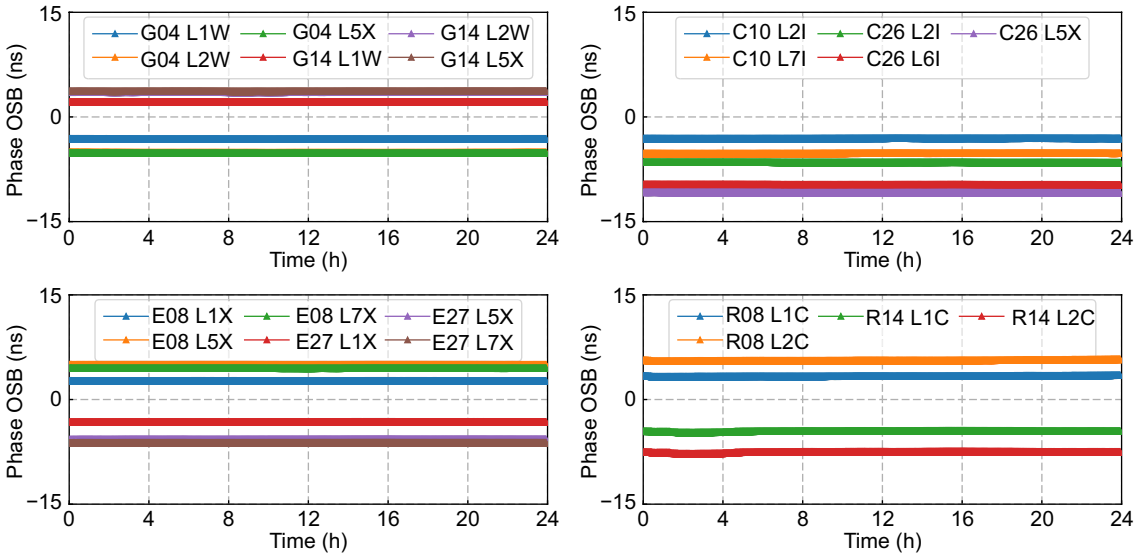

Fig. 8 Phase OSBs for GPS, BDS, Galileo, and GLONASS on DOY 254, 2021

observation noises (Li et al., 2019). However, propably due to immature models and imperfect orbits, the stability of BDS code/phase OSBs cannot fully reflect the advantages of BDS-3 signals.

IFCB evaluation

IFCB is composed of code IFCB (CIFCB) and PIFCB. Since CIFCB can be obtained from a linear combination of OSB/DCB (Fan et al., 2019), and PIFCBs of Galileo and BDS satellites are so small that can be ignored (Pan et al., 2017), only GPS PIFCBs are evaluated here. PIFCB series of GPS Block IIF and the new Block III satellites from DOY 256 to 265, 2021 are displayed in Fig. 9. As can be seen, the peak-to-peak amplitude of a GPS BLOCK IIF satellite is generally over 10 cm, especially the value for G09 satellite is larger than 21 cm. GPS III satellites show a smaller variation of less than 3 cm, manifesting that the L5 carrier phase observations of GPS III satellites are barely affected by PIFCB errors. Figure 10 shows the RMS statistics of the estimated GPS PIFCBs. The RMSs of GPS III satellites are generally smaller than 1 cm, indicating that PIFCB errors of GPS III satellites can be ignored.

Table 7 Average STDs of the estimated phase OSBs on DOY 254, 2021

System	Band	STD (ns)
GPS	L1	0.011
	L2	0.015
	L5	0.014
BDS	B1I	0.031
	B2I	0.035
	B3I	0.038
	B2a	0.043
Galileo	E1	0.010
	E5a	0.013
	E5b	0.013
GLONASS	L1	0.074
	L2	0.096

PPP evaluation

To further evaluate the overall performance of GRT orbit, clock, and bias products, dual-/triple-frequency PPP AR on DOY 128, 2021 is carried out. PPP experiments with CODE and WHU products are also conducted for comparison. The three PPP solutions are listed in Table 8, and 16 global-distributed stations are employed. In PPP processing, IF combinations of code and phase observations are used, and the mask elevation is set to 7°. GPS IFCB is adopted in triple-frequency PPP processing. The positioning performance is mainly evaluated from three perspectives, i.e., positioning accuracy, convergence time, and Time to First Fixed (TTFF).

Taking the coordinates of IGS weekly solution as references, positioning accuracies in east, north, and up components are summarized in Fig. 11. The 24-h average positioning accuracy of fixed solutions in horizontal and vertical directions is better than 1 cm. It can be seen that AR improves positioning accuracy significantly,

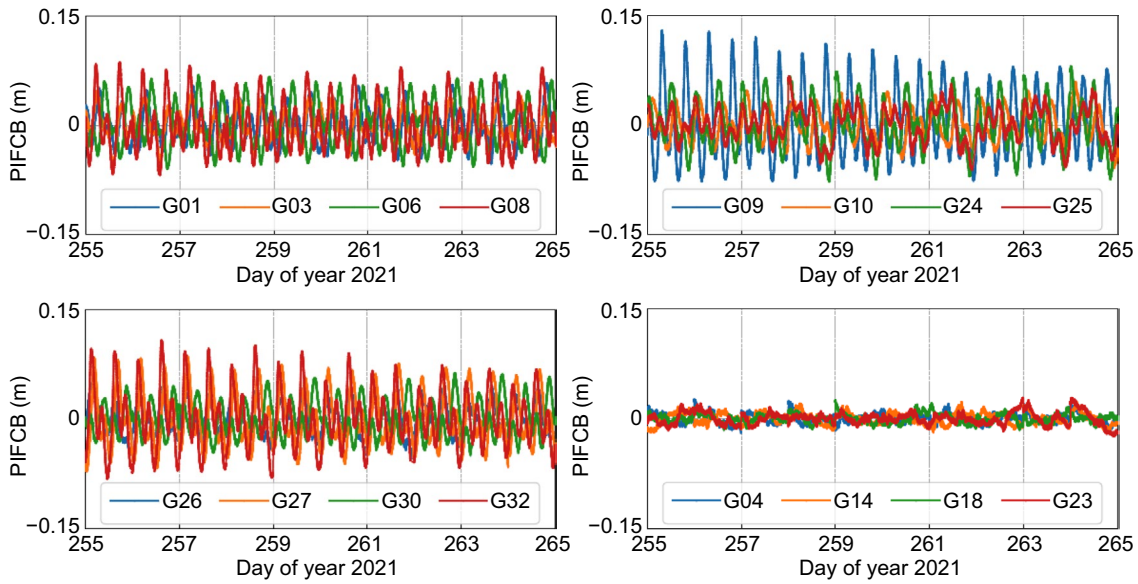

Fig. 9 GPS PIFCBs of GPS Block IIF (blue dots) and GPS III (coral dots) satellites on DOYs 256–265, 2021

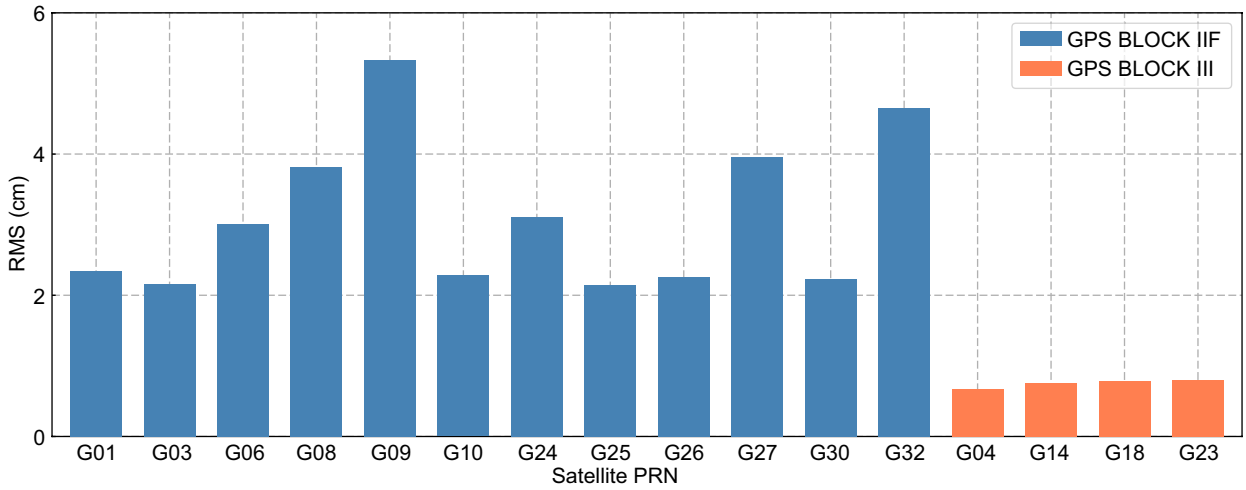

Fig. 10 RMSs of the estimated GPS PIFCBs on DOYs 256–266, 2021

Table 8 GNSS products used in PPP processing

Institution name	Bias product	IFCB product	Orbit product		Clock product	
			Type	Interval (s)	Type	Interval (s)
IAC	OSB	GPS IFCB	Precise orbit	300	Precise clock	30
CODE	OSB	GPS IFCB	Final orbit	300	Ambiguity-fixed clock	30
WHU	OSB	GPS IFCB	Final orbit	300	Modified phase clock	30

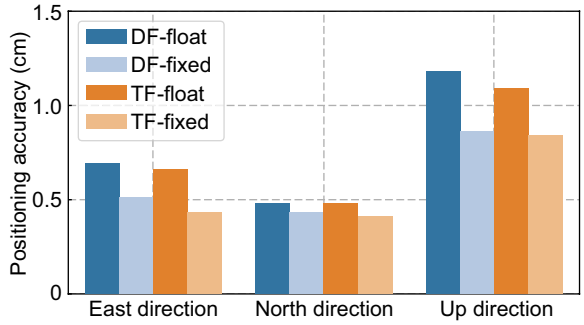

Fig. 11 Average 24 h positioning accuracy of IAC quad-system PPP solutions. DF-float, DF-fixed, TF-float, TF-fixed denote dual- and triple-frequency PPP float and fixed solutions, respectively

Table 9 Average convergence time of IAC/CODE/WHU solutions

Institution name	Convergence time of different solutions (min)			
	DF-float	DF-fixed	TF-float	TF-fixed
IAC	8.58	6.50	8.28	6.11
CODE	8.75	6.74	8.30	6.43
WHU	8.50	6.60	8.23	6.10

especially in east and up directions. Compared with the float solutions, positioning accuracy of dual-frequency fixed solution is improved by 26%, 10%, and 27%, while that of triple-frequency solution is improved by 35%, 15%, and 23% in east, north and up directions, respectively.

The convergence time refers to the time needed for positioning errors at 10 consecutive epochs less than 5 and 10 cm in horizontal and vertical components, respectively. Table 9 presents the average convergence time of IAC/CODE/WHU solutions. Figure 12 shows the positioning errors for IAC solution in 0–3 h at station STR2 with the observations of GPS only, GPS + BDS, GPS + BDS + Galileo and GPS + BDS + Galileo + GLONASS. The performance of convergence time for IAC, CODE, and WHU solutions is comparable. It can be seen from the faster convergence shown in this figure that GRT bias products can take full advantage of multi-frequency and multi-system observations. Moreover, AR shortens the convergence time of dual- and triple-frequency PPP solutions for IAC from 8.58 to 6.50 min, and from 8.28 to 6.11 min, with improvement of 24.2% and 26.2%, respectively.

TTFF is defined as the time taken to fix ambiguity successfully for 5 consecutive epochs. IAC pioneers to provide GLONASS phase OSB and multi-frequency phase

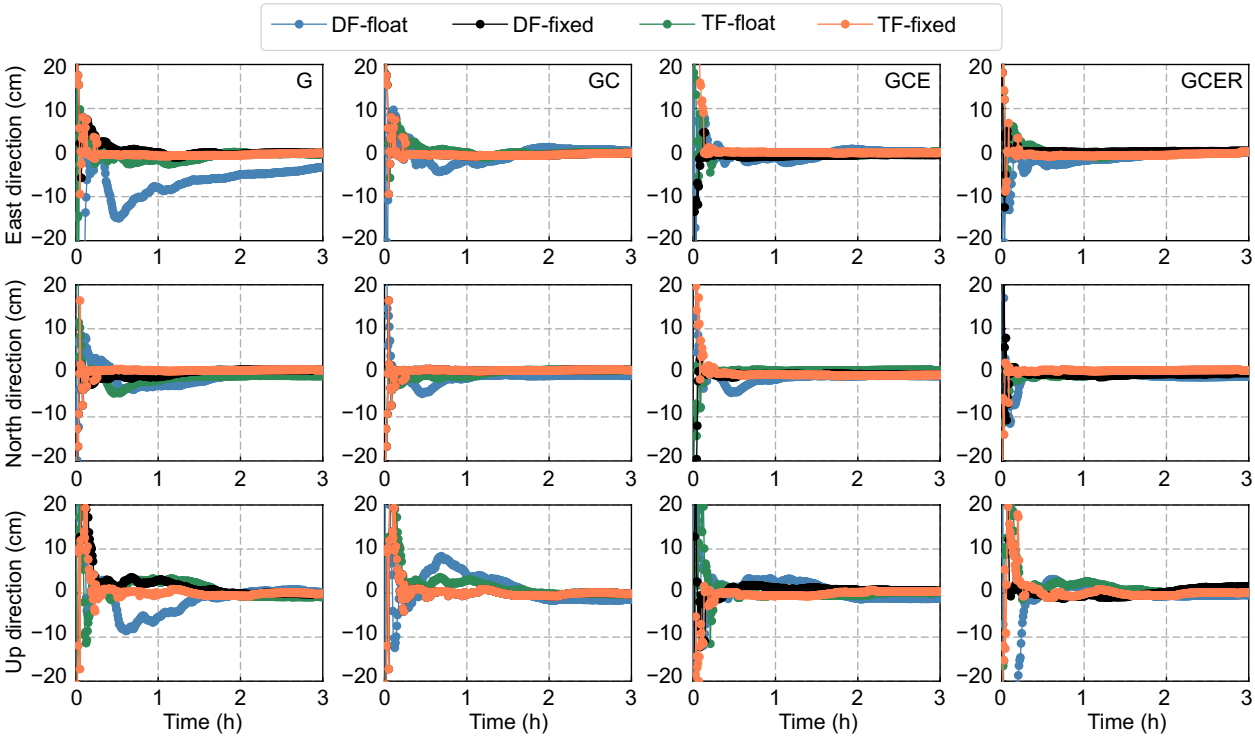

Fig. 12 Positioning errors in east, north, and up components with G/GC/GCE/GCER observations at station STR2

Table 10 Average TTFF of IAC/CODE/WHU fixed solutions

Institution name	TTFF of different solutions (min)	
	DF-fixed	TF-fixed
IAC	6.11	4.25
CODE	6.54	4.74
WHU	6.18	4.30

OSB, so that both GLONASS AR and triple-frequency fixed solution can be realized. As can be seen from Table 10, the TTFF performance of IAC is slightly better than that of CODE and WHU. With GRT products, the average TTFF is shortened by 32.3% from dual- to triple-frequency fixed solution. This can be attributed to the increase in observations and confirms the superiority of the GRT multi-frequency and multi-system bias product.

Real-time service

Real-time service status

To meet the needs of time-critical applications like real-time positioning (Zuo et al., 2021), atmosphere remote sensing (Ding et al., 2017), natural disaster monitoring and early warning (Samper & Merino, 2013), etc., IGS established the Real-Time Working Group (RTWG) in 2001. Later in 2013, IGS officially launched the Real-Time Service (RTS) (Elsobeiey & Al-Harbi, 2016). The implementation of real-time services has gained significant achievement over the past decades. IAC provides RTS to comply with the development of real-time GNSS as well. Table 11 summarizes the information of RTS for IGS and IAC as of Jan. 2022. Among them, CAS, CNES/CLS, DLR, GFZ, GMV, WHU, and IAC provide the quad-system real-time satellite corrections with an interval of 5 s.

Table 11 Summary of real-time orbit and clock products as of January 2022

Institution name	System	Ultra-rapid orbit
DLR	G, C, E, R, J	IGV/CODE/DLR orbits
GFZ	G, C, E, R	GFZ orbits
CAS	G, C, E, R	GFZ orbits
CNES/CLS	G, C, E, R	GFZ orbits
GMV	G, C, E, R	GMV orbits
WHU	G, C, E, R	IGU (GPS) orbits and WHU orbits
BKG	G, E, R	CODE orbits
ESA	G	IGU (GPS) orbits
SHAO	G	IGU (GPS) orbits
NRCan	G	NRCan orbits
IAC	G, C, E, R	GRT ultra-rapid orbits

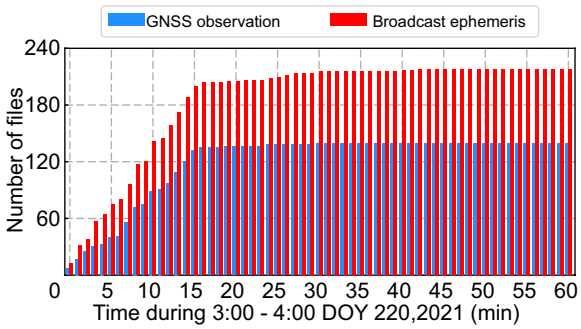

Fig. 13 The number of hourly observation files and ephemerides of CDDIS

Ultra-rapid orbit determination

For real-time orbit/clock generation, the orbit is predicted first and then the clock is estimated with orbit fixed, i.e., the prediction-estimation mode is applied (Kuang et al., 2019). The innovations made by IAC and differences between ultra-rapid and post-processed orbit determination are emphasized in this section.

Firstly, in ultra-rapid orbit determination, observations and broadcast ephemerides are obtained by merging hourly observation files and navigation ephemerides, respectively. To download as complete data as possible in the shortest time, it is necessary to count the hourly file transfer time on data center. Figure 13 shows the time series of the two kinds of hourly files on Crustal Dynamics Data Information System (CDDIS). It can be seen that the number of hourly observation files and navigation ephemerides exceeds 160 and 120, respectively, in 15 min, and then keeps almost constant. Therefore, the recommended downloading time is about 15 min, satisfying both the basic orbit determination requirements and subsequent computation time.

Secondly, unlike the 6 h update interval of IGU orbit (3:00–21:00 Universal Time Coordinated), GRT ultra-rapid orbit is released every 2 h from 0:00 to 22:00. The higher update rate is to capture the orbit model variations timely, which improves the orbit prediction, especially for new systems with immature orbit model (Deng et al., 2016). Besides, the predicted orbit accuracy is deteriorated with an increase in prediction time. To relieve computation burden caused by high updating rate, efficiency optimization is necessary. In addition to reducing the number of stations to about 100, multiprocessing is utilized in data downloading and processing. The four satellite systems are calculated in three groups parallelly, namely, GPS + BDS, GPS + Galileo, and GPS + GLONASS. GPS orbit estimated in the GPS + Galileo group is adopted in the final orbit product. In this way, the whole orbit determination can be completed in 1.6–1.7 h.

Finally, GRT ultra-rapid orbit is composed of 24 h observed arc and 24 h predicted arc. Instead of directly integrating and predicting orbit, an innovative step is added before orbit extrapolation. That is, the orbit at the same time of the previous day is applied in orbit fitting with the observed arc to get more accurate satellite state information at the reference time. Afterwards, a 48-h forward integration is employed to obtain both the observed and predicted orbits. This method adds the observations of the previous day in a sense of extending the observation arc to 48 h. As was verified by Li et al. (2019), the 48 h observations can effectively improve the accuracy of ultra-rapid predicted orbit. This strategy effectively ameliorates the accuracy of predicted orbit without increasing too much computation time.

Real-time clock estimation

Real-time clock estimation requires high timeliness. This section focuses on the key points employed by IAC to achieve both superior efficiency and high precision of real-time clock estimation.

Stable real-time data stream is the prerequisite for real-time clock estimation. More than 80 IGS/MGEX stations are carefully selected with a good tracking status for all constellations. Based on the real-time observations, broadcast ephemeris stream, and predicted orbits, real-time clock can be estimated. Efficient quality control methods are indispensable to detect and eliminate abnormal errors in real-time observations. In this contribution, a recursive Detection, Identification, and Adaptation (DIA) procedure is adopted for dynamically detecting and removing gross errors (Teunissen, 2017). Firstly, the STD of unit weight is used to detect the existence of outliers, and then the IGGIII (Institute of Geodesy and Geophysics, Yang et al., 2002) scheme is employed to identify abnormal residuals. Finally, the corresponding observations are downweighed or eliminated.

The computational burden is also a critical issue. In real-time clock estimation, the undifferenced method is adopted to accelerate the solution convergence and avoid sacrifice of useful information. However, this method increases the estimated parameters and further increase the computation burden (Liu et al., 2019; Odijk et al., 2016). Moreover, large-scale matrix calculation in GNSS data processing is time-consuming. With the support of computer hardware and software algorithms, the efficiency problem caused by numerous estimated parameters and frequent matrix operations is solved by the following approaches. Firstly, the estimator of sequential least squares is applied, so that sequential measurement processing and updating can be realized. Secondly, considering the independence of observations, the Open Multi-Processing (OpenMP, Kuang et al., 2019) provides another resolution. Based on the multi-core computer or supercomputer, data preprocessing and construction of normal equation for different stations can be conducted in a station-based parallel way (Wang et al., 2017). Besides, the linear algebra matrix libraries in Open Basic Linear Algebra Subprograms (OpenBLAS) are fully utilized for solving high-dimensional linear equations.

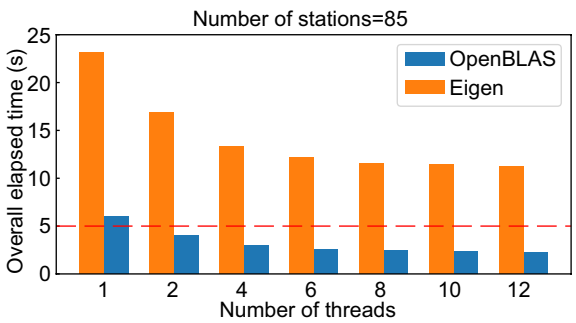

Fig. 14 Overall elapsed time per epoch using OpenBLAS or Eigen with various number of threads

Figure 14 summarizes the overall elapsed time for different strategies. The computation time is shortened by 33.5–62.0% compared with single thread, with number of threads from 2 to 12 at interval of 2. Besides, OpenBLAS significantly reduces computation time with reference to traditional matrix libraries provided by Eigen. With OpenBLAS, the computation efficiency is improved by 73.8%-79.6% with different number of threads shown in the figure. When the number of threads reaches 6, the computation time hardly changes and the average time per epoch is less than 2.6 s with OpenBLAS.

Assessment of real-time services

In this section, the RTS is evaluated comprehensively. The internal accuracy of ultra-rapid orbits is first assessed. Then the consistency between GRT real-time orbit/clock and GBM final orbit/clock products is examined. Subsequently, the observations from three stations are collected to conduct RTPPP for further RTS evaluation.

Ultra-rapid orbit assessment

The discrepancy between the overlapping neighboring orbits reflects their accuracy. Because of the 2-h update interval of ultra-rapid orbits, the differences between 22-h observed and 2-h predicted orbits are calculated. Figure 15 presents the results in along-, cross-track, and radial components from DOY 331 to 360, 2021. Since the predicted orbit plays an important role in real-time clock estimation, its accuracy is analyzed. On average, the orbit differences of predicted arc are 0.70 cm, 0.52 cm, and 1.02 cm larger than observed arc in along-, cross-track

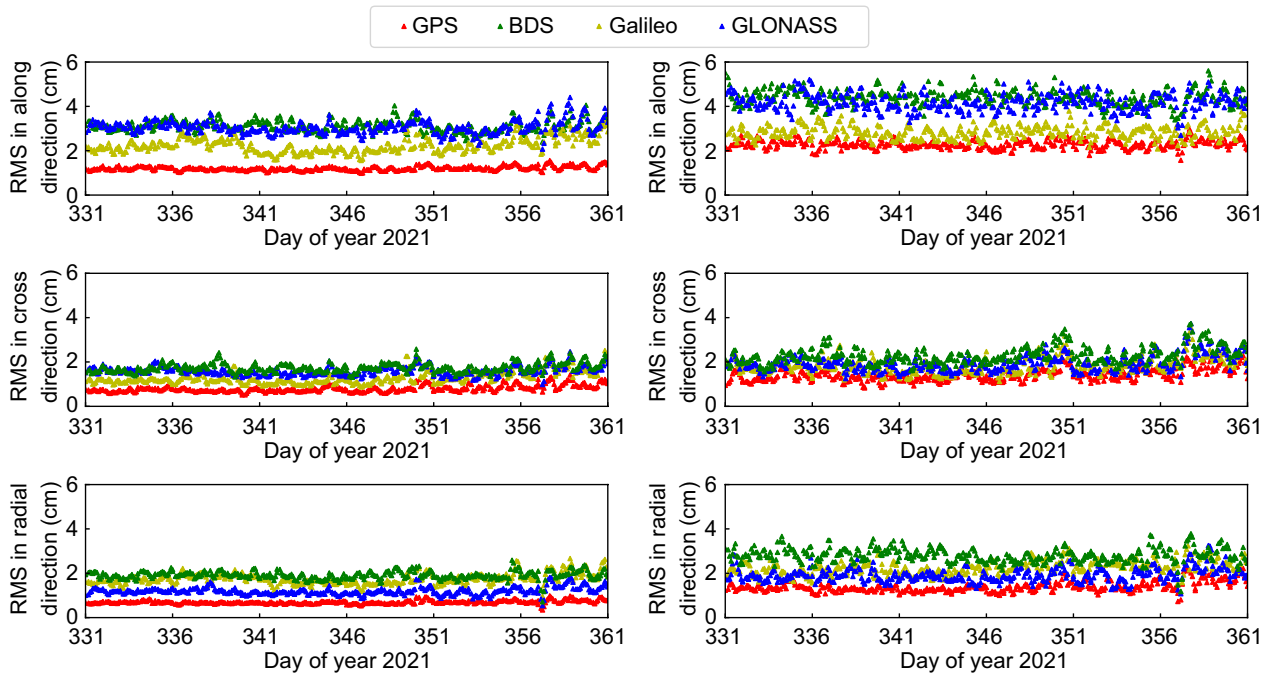

Fig. 15 RMSs of observed (left) and predicted (right) orbit overlap differences in along-, cross-track, and radial components

Table 12 Average orbit differences between IAC/WHU ultra-rapid orbits and GBM final orbits

Institution name	System	Orbit differences (observed/predicted (cm))			
		Along-track direction	Cross-track direction	Radial direction	3D
IAC (Old)	GPS	2.28/2.96	1.96/2.47	2.53/2.65	3.93/4.68
	BDS	5.80/5.86	4.84/5.07	4.75/4.81	8.92/9.12
	Galileo	3.01/4.80	2.63/3.02	3.66/3.96	5.42/6.92
	GLONASS	5.47/5.67	5.88/5.98	4.91/4.88	9.41/9.58
IAC (New)	GPS	2.06/2.80	1.88/2.29	1.61/2.14	3.22/4.20
	BDS	5.26/5.64	4.48/4.45	4.64/4.28	8.32/8.36
	Galileo	2.95/3.82	2.49/2.88	3.40/3.56	5.14/5.96
	GLONASS	5.25/5.44	5.74/5.72	4.98/4.89	9.24/9.29
WHU	GPS	1.82/3.07	1.74/1.96	2.05/2.29	3.25/4.30
	BDS	5.9/5.85	4.67/4.68	3.95/3.52	8.50/8.28
	Galileo	2.51/4.23	2.19/3.16	4.11/4.04	5.29/6.65
	GLONASS	4.15/3.60	4.86/5.74	6.49/5.95	9.11/9.02

and radial directions, respectively. Among the four constellations, GPS predicted orbits are the best, with an average 3D RMS of 3.32 cm, followed by Galileo 4.43 cm, GLONASS 5.42 cm, and BDS 6.25 cm.

Furthermore, GRT ultra-rapid orbits during the 30 d are compared with GBM orbits at 300 s sampling rate. The results with the modified orbit prediction are denoted as "IAC (New)", and the results with direct orbit integration are denoted as "IAC (old)". It can be seen that both observed and predicted orbits of IAC (new) show higher accuracy than IAC (old). The 3D predicted orbit accuracy for the four constellations is improved by 2.9–9.6 mm. This suggests the aforementioned orbit prediction strategy is effective.

Moreover, orbit differences between the ultra-rapid orbit of WHU and GBM final orbit over the same period are also summarized in Table 12. Basically, the ultra-rapid orbit accuracy of IAC (New) is comparable to that of WHU.

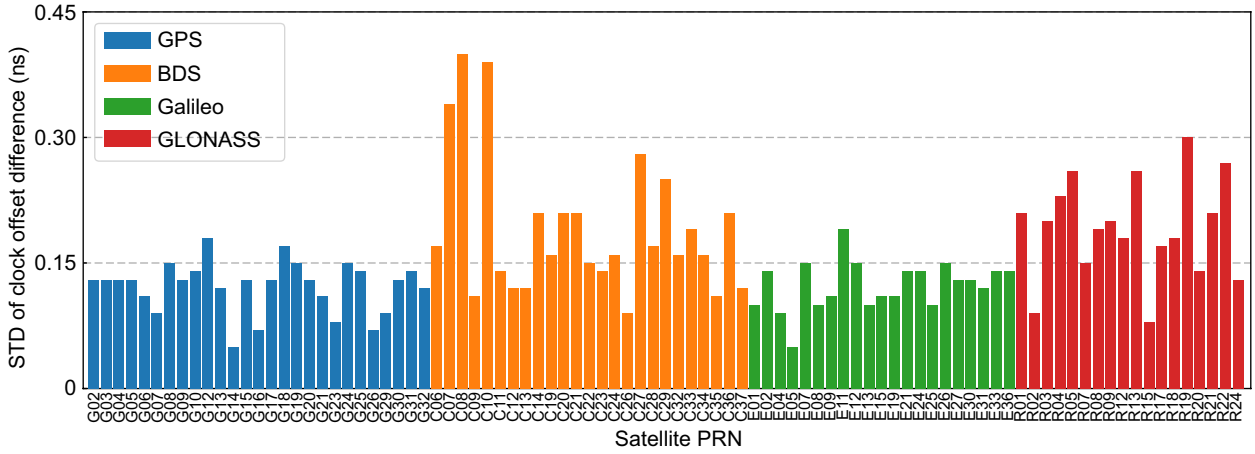

Fig. 16 STDs of GRT real-time clock compared with GBM final products

GPS orbits show the best agreement with respect to GBM orbits among the four systems, followed by Galileo and BDS. GLONASS orbit shows the worst consistency due to the difficulty in ambiguity fixing. For the four systems, the differences between observed arc and predicted arc are within 1.5 cm, indicating that the predicted orbits diverge slowly and meet the needs of real-time clock estimation.

Real-time clock assessment

Figure 16 shows the average STDs of clock differences with respect to GBM final products from DOY 357 to 359, 2021. G01, C16, E06, and R06 are taken as the reference clock for GPS, BDS, Galileo, and GLONASS, respectively. It can be seen that STDs for most GPS and Galileo satellites are within 0.15 ns, and average STDs of 0.12 ns are achieved for both GPS and Galileo. The accuracy of BDS real-time clock is slightly worse with an average STD of 0.19 ns due to the fact that most BDS-2 IGSOs have STDs larger than 0.30 ns. The major reason may be the lack of IGSO observations, low-precision orbits, and immature clock models. GLONASS has the performance similar to BDS with an average STD of 0.19 ns. The clock comparison results are generally consistent with the orbit comparison results. Note that the quality of real-time orbit, especially the predicted one, plays an important role in real-time clock estimation. Considering that there are still some discrepancies between predicted and observed orbits, the performance of real-time clock can be further improved with the improvement of predicted orbit accuracy and convergence.

Real-time PPP validation

RTPPP is carried out to further verify the stability and reliability of RTS. With real-time satellite corrections, RTPPP is conducted at 6 tracking stations, and the positioning performance is intuitively displayed for the IAC registered users at http://igmas.users.sgg.whu.edu.cn/monitor/clk/rtppp.

Figure 17 displays the 24-h RTPPP positioning errors with GRT real-time satellite corrections at stations JFNG, HOB2, and ALIC on DOYs 113–114, 2022. It can be seen that after convergence, the positioning accuracy in east, north, and up components are almost within ± 10 cm. RTPPP positioning accuracy and convergence time of the three stations with GRT, GFZ, and CNES/CLS real-time products are given in Table 13. Overall, IAC reaches comparable RTPPP performance to GFZ and CNES/CLS. For IAC, the average positioning errors in east, north, and up directions are 1.95, 1.37, and 3.89 cm, respectively, and the average convergence time is 16.97 min. Both the good positioning accuracy and fast convergence indicate the high quality of the multi-GNSS RTS, meeting the requirements of real-time applications. Nevertheless, there are discontinuities in RTPPP results. This problem is caused by the interruption of real-time data stream, and it will be gradually optimized later.

Conclusions

The development of multi-GNSS increases the number of available satellites and signal resources, and optimizes the spatial geometry. However, current GNSS products are inadequate to support some new frequencies or systems. With the support of GREAT software, iGMAS Wuhan IAC provides a complete suite of precise/real-time products to meet different requirements of GNSS applications, and alleviates the problem of insufficient multi-frequency and multi-system products. Following an analysis of current GNSS products/services, this

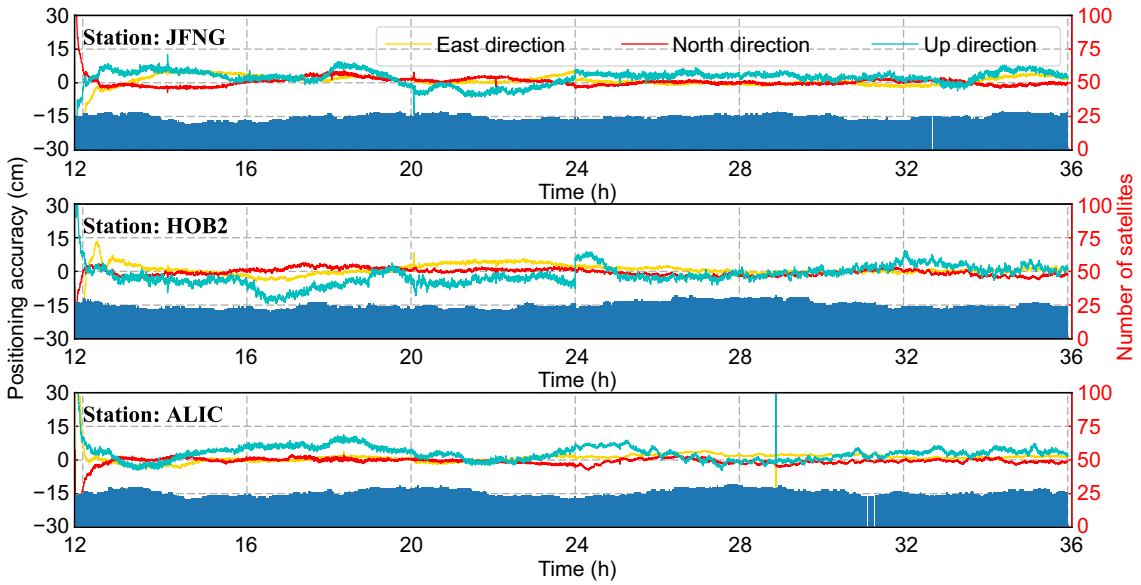

Fig. 17 RTPPP positioning errors in east, north, and up components at stations JFNG, HOB2, and ALIC on DOYs 113–114, 2022

Table 13 RTPPP positioning accuracy and convergence time

Station	Positioning accuracy of different institutions (east/north/up (cm))			Convergence time of different institutions (min)		
	GRT	GFZ	CNES/CLS	GRT	GFZ	CNES/CLS
JFNG	2.07/1.82/3.38	1.39/0.94/4.10	2.12/1.38/3.88	16.08	17.33	18.83
HOB2	2.40/1.19/4.22	1.46/2.32/3.35	2.04/1.69/4.14	17.75	17.50	11.00
ALIC	1.39/1.09/4.07	1.47/1.70/4.08	1.71/1.63/3.39	17.08	10.05	20.60
Mean	1.95/1.37/3.89	1.44/1.65/3.84	1.96/1.57/3.80	16.97	15.11	16.81

article focuses on the product generation, innovations, and improvements of IAC, and verifies the products in terms of several aspects.

In post-processed products, IAC pioneers to provide the quad-system multi-frequency phase OSB and GPS IFCB. The formulas and strategies of bias estimation are introduced in detail. Then, GRT orbit/clock products are compared with the precise orbit/clock products of several well-recognized institutions. For GPS, BDS, Galileo, and GLONASS, the average 3D orbit differences are 2.11, 7.30, 3.39, and 5.79 cm, respectively. The average clock comparison results are within 0.06 ns for GPS and Galileo, and around 0.08 ns for BDS and GLONASS. Afterwards, OSB and IFCB products are assessed, and they exhibit long-term stability. The overall performance of orbit, clock, and bias products is verified by PPP AR. The positioning accuracy is better than 1 cm in horizontal and vertical directions, convergence time is within 6.50 min, and TTFF is less than 6.20 min. In addition, the convergence speed is improved by around 25% from float to fixed solutions, demonstrating the reliability of multi-frequency bias product.

For real-time services, key strategies and innovations are specifically introduced. In ultra-rapid orbit determination, the modified orbit prediction strategy improves the 3D orbit accuracy with reference to GBM final orbit by 2.9–9.6 mm for the four constellations. For real-time clock estimation, the multi-thread strategy and high-performance matrix library employed significantly relieve the computation burden. When the number of threads reaches 6, the calculation time per epoch with OpenBLAS is less than 2.6 s, which is shortened by 57.4%. The average STDs of clock differences compared with GBM final clock products are 0.12, 0.19, 0.12, and 0.19 ns for GPS, BDS, Galileo and GLONASS, respectively. With real-time satellite corrections and observations, RTPPP is conducted to further verify the reliability of RTS. The average positioning errors are within 2.0 and 4.0 cm in horizontal and vertical directions, respectively, and the average convergence time is 16.97 min.

Acknowledgements
The numerical calculations in this paper have been done on the supercomputing system in the Supercomputing Center of Wuhan University.

Author contributions
XL, QW conceived the idea and wrote the paper; JW and YY assisted in data acquisition; YX, XG and ZW helped with the article writing and revision. All authors read and approved the final manuscript.

Funding
This study is financially supported by the National Natural Science Foundation of China (No. 41974027), the National Key Research and Development Program of China (2021YFB2501102) and the Sino-German mobility programme (Grant No. M-0054).

Availability of data and materials
The datasets used and analyzed in this study are available from the corresponding author on reasonable request.

Declarations

Competing interests
The authors declare that they have no competing interests.

Received: 5 March 2022 Accepted: 14 August 2022
Published online: 26 September 2022

References

Arnold, D., Meindl, M., Beutler, G., et al. (2015). CODE's new solar radiation pressure model for GNSS orbit determination. *Journal of Geodesy, 89*, 775–791. https://doi.org/10.1007/s00190-015-0814-4

Banville, S., Geng, J., Loyer, S., et al. (2020). On the interoperability of IGS products for precise point positioning with ambiguity resolution. *Journal of Geodesy, 94*, 10. https://doi.org/10.1007/s00190-019-01335-w

Chen, J. P., Wu, B., Hu, X. G., et al. (2012). *SHA: The GNSS analysis center at SHAO. Lecture Notes in Electrical Engineering,* 160 LNEE, 213–221.

Chen, J., Zhang, Y., Zhou, X., et al. (2014). GNSS clock corrections densification at SHAO: From 5 min to 30 s. *Science China Physics, Mechanics and Astronomy, 57*, 166–175. https://doi.org/10.1007/s11433-013-5181-7

Chen, K., Xu, T., Chen, G., Li, J., & Yu, S. (2015). The orbit and clock combination of iGMAS analysis centers and the analysis of their precision. *In: Proceedings of the 6th China satellite navigation conference (CSNC)* (Vol. 341, pp. 421–438). LNEE. Xi'an. https://doi.org/10.1007/978-3-662-46635-3_36

Dach, R., Schaer, S., Lutz, S., Arnold, D., Bock, H., Orliac, E., et al. (2015). CODE analysis center technical report 2014. In R. Dach, & Y. Jean (Eds.), *International GNSS Service: Technical Report 2014, (AIUB)* (pp. 21–34). IGS Central Bureau. https://doi.org/10.7892/boris.80302.

Deng, Z., Fritsche, M., Uhlemann, M., et al. (2016). *Reprocessing of GFZ Multi-GNSS product GBM, IGS Workshop 2016.*

Ding, W., Teferle, F. N., Kazmierski, K., et al. (2017). An evaluation of real-time troposphere estimation based on GNSS Precise Point Positioning. *Journal of Geophysical Research: Atmospheres, 122*(5), 2779–2790.

Dow, J. M., Neilan, R. E., & Rizos, C. (2009). The International GNSS service in a changing landscape of global navigation satellite systems. *Journal of Geodesy, 83*(3–4), 191–198. https://doi.org/10.1007/s00190-008-0300-3

Elsobeiey, M., & Al-Harbi, S. (2016). Performance of real-time Precise Point Positioning using IGS real-time service. *GPS Solutions, 20*(3), 565–571. https://doi.org/10.1007/s10291-015-0467-z

Fan, L., Shi, C., Li, M., et al. (2019). GPS satellite inter-frequency clock bias estimation using triple-frequency raw observations. *Journal of Geodesy, 93*(12), 2465–2479. https://doi.org/10.1007/s00190-019-01310-5

Folkner, W., Williams, J., & Boggs, D. (2009). The planetary and lunar ephemeris DE 421 (IPN Progress Report 42–178). Jet Propulsion Laboratory.

Geng, J., Chen, X., Pan, Y., et al. (2019). A modified phase clock/bias model to improve PPP ambiguity resolution at Wuhan University. *Journal of Geodesy, 93*(10), 2053–2067. https://doi.org/10.1007/s00190-019-01301-6

Guo, F., Li, X., Zhang, X., et al. (2017). Assessment of precise orbit and clock products for Galileo, BeiDou, and QZSS from IGS Multi-GNSS Experiment (MGEX). *GPS Solutions, 21*(1), 279–290. https://doi.org/10.1007/s10291-016-0523-3

Guo, J., Xu, X., Zhao, Q., et al. (2016). Precise orbit determination for quad-constellation satellites at Wuhan University: Strategy, result validation, and comparison. *Journal of Geodesy, 90*(2), 143–159. https://doi.org/10.1007/s00190-015-0862-9

Hatch, R. (1983). The synergism of GPS code and carrier measurements. IN: Proceedings of the International Geodetic Symposium on Satellite Doppler Positioning, 3rd, Volume 2 (A84-18251 06-42). Las Cruces, NM, New Mexico State University, 1213–1231.

Kuang, K., Zhang, S., & Li, J. (2019). Real-time GPS satellite orbit and clock estimation based on OpenMP. *Advances in Space Research, 63*(8), 2378–2386.

Li, H., Zhou, X., Wu, B., et al. (2012). Estimation of the inter-frequency clock bias for the satellites of PRN25 and PRN01. *Science China Physics, Mechanics and Astronomy, 55*(11), 2186–2193. https://doi.org/10.1007/s11433-012-4897-0

LI, T., Wang, J., & Laurichesse, D. (2014). Modeling and quality control for reliable precise point positioning integer ambiguity resolution with GNSS modernization. *GPS Solutions, 18*(3), 429–442. https://doi.org/10.1007/s10291-013-0342-8

Li, X., Chen, X., Ge, M., et al. (2019). Improving multi-GNSS ultra-rapid orbit determination for real-time precise point positioning. *Journal of Geodesy, 93*(1), 45–64. https://doi.org/10.1007/s00190-018-1138-y

Li, X., Han, X., Li, X., et al. (2021). GREAT-UPD: An open-source software for uncalibrated phase delay estimation based on multi-GNSS and multi-frequency observations. *GPS Solutions, 25*(2), 66. https://doi.org/10.1007/s10291-020-01070-2

Li, X., Zhu, Y., Zheng, K., Yuan, Y., Liu, G., & Xiong, Y. (2020). Precise orbit and clock products of Galileo, BDS and QZSS from MGEX since 2018: Comparison and PPP validation. *Remote Sensing, 12*(9), 1415. https://doi.org/10.3390/rs12091415

Liu, T., Zhang, B., Yuan, Y., et al. (2019). An efficient undifferenced method for estimating multi-GNSS high-rate clock corrections with data streams in real time. *Journal of Geodesy, 93*(9), 1435–1456. https://doi.org/10.1007/s00190-019-01255-9

Loyer, S., Perosanz, F., Mercier, F., et al. (2012). Zero-difference GPS ambiguity resolution at CNES–CLS IGS Analysis Center. *Journal of Geodesy, 86*(11), 991–1003. https://doi.org/10.1007/s00190-012-0559-2

Mayer, V., Springer, T., Schoenemann, E., Enderle, W. (2018). *Presentation of ESA's Public Multi-GNSS Products. Geodetic Week 2018, Intergeo Congress, October 16–18*, Frankfurt, Germany.

Melbourne, W. G. (1985). The case for ranging in GPS-based geodetic systems. In: Proceedings of the 1st International Symposium on Precise Positioning with the Global Positioning System, edited by Clyde Goad. Rockville, Maryland, U. S. Department of Commerce, 403–412.

Montenbruck, O., Hauschild, A., & Steigenberger, P. (2014). Differential code bias estimation using multi-GNSS observations and global ionosphere maps. *Journal of the Institute of Navigation, 61*(3), 191–201. https://doi.org/10.1002/navi.64

Montenbruck, O., Hugentobler, U., Dach, R., et al. (2012). Apparent clock variations of the Block IIF-1 (SVN62) GPS satellite. *GPS Solutions, 16*(3), 303–313. https://doi.org/10.1007/s10291-011-0232-x

Montenbruck, O., Steigenberget, P., Prangr, L., Deng, Z., Zhao, Q., Perosanz, F., Romero, I., Noll, C., Stürze, A., Weber, G., Schmid, R., MacLeod, K., & Schaer, S. (2017). The Multi-GNSS Experiment (MGEX) of the International GNSS Service (IGS)—Achievements, prospects and challenges. *Advances in Space Research, 59*(7), 1671–1697. https://doi.org/10.1016/j.asr.2017.01.011

Nikolaos, P. K., Simon, H. A., Steve, K. C., et al. (2012). The development and evaluation of the Earth Gravitational Model 2008 (EGM2008). *Journal of Geophysical Research: Solid Earth, 117*, B04406.

Odijk, D., Zhang, B., Khodabandeh, A., et al. (2016). On the estimability of parameters in undifferenced, uncombined GNSS network and PPP-RTK user models by means of S-system theory. *Journal of Geodesy, 90*(1), 15–44. https://doi.org/10.1007/s00190-015-0854-9

Pan, L., Zhang, X., Li, X., et al. (2017). Characteristics of inter-frequency clock bias for Block IIF satellites and its effect on triple-frequency GPS precise point positioning. *GPS Solutions, 21*(2), 811–822. https://doi.org/10.1007/s10291-016-0571-8

Petit, G., & Luzum, B. (2010). IERS Conventions (2010), IERS Technical Note, 36.

Prange, L., Orliac, E., Dach, R., et al. (2017). CODE's five-system orbit and clock solution—The challenges of multi-GNSS data analysis. *Journal of Geodesy, 91*, 345–360. https://doi.org/10.1007/s00190-016-0968-8
Rebischung, P., Schmid, R., & Herring, T. (2016). Upcoming switch to IGS14/igs14.atx. IGSMAIL-7399. Retrieved from https://lists.igs.org/pipermail/igsmail/2016/001233.html.
Rovira-Garcia, A., Juan, J. M., Sanz, J., et al. (2021). A multi-frequency method to improve the long-term estimation of GNSS clock corrections and phase biases. *Navigation, 68*, 815–828. https://doi.org/10.1002/navi.453
Samper, L., & Merino, M. (2013). Advantages and drawbacks of the Precise Point Positioning (PPP) technique for earthquake, tsunami prediction and monitoring. In: Proceedings of the ION 2013 pacific PNT meeting, Volume 8900, No. 6. Honolulu, Hawaii, 9–26.
Schaer, S., Villiger, A., Arnold, D., et al. (2021). The CODE ambiguity-fixed clock and phase bias analysis products: Generation, properties, and performance. *Journal of Geodesy, 95*, 81. https://doi.org/10.1007/s00190-021-01521-9
Springer, T., Dilßner, F., Schoenemann, E., Zandbergen, R., & Enderle, W. (2017). The ESA/ESOC analysis Centre progress and improvements. In *IGS workshop 2017*, Paris, France.
Steigenberger, P., & Montenbruck, O. (2019). Consistency of MGEX orbit and clock products. *Engineering, 6*(8), 898–903. https://doi.org/10.1016/j.eng.2019.12.005
Teunissen, P. J. G. (2017). Distributional theory for the DIA method. *Journal of Geodesy, 92*, 59–80. https://doi.org/10.1007/s00190-017-1045-7
Uhlemann, M., Gendt, G., Ramatschi, M., & Deng, Z. (2014). GFZ global multi-GNSS network and data processing results. In P. Willis (Ed.), IAG 150 Years. *International Association of Geodesy Symposia, vol 143.* (pp. 1–7). Springer, Cham. https://doi.org/10.1007/1345_2015_120.
Villiger, A., Schaer, S., Dach, R., et al. (2019). Determination of GNSS pseudo-absolute code biases and their long-term combination. *Journal of Geodesy, 93*(3–4), 1487–1500. https://doi.org/10.1007/s00190-019-01262-w
Wang, C., Shi, C., & Zhang, H. (2017). *WHU ionosphere products and parallel computing for global ionospheric modeling*, IGS Workshop 2017.
Wang, N., Yuan, Y., Li, Z., et al. (2016). Determination of differential code biases with multi-GNSS observations. *Journal of Geodesy, 90*(3), 209–228. https://doi.org/10.1007/s00190-015-0867-4
Wanninger, L., Beer Wanninger, L., & Wallstab-Freitag, S. (2007). Combined processing of GPS, GLONASS, and SBAS code phase and carrier phase measurements. In: Proceedings of the 20th International Technical Meeting of the Satellite Division of The Institute of Navigation (ION GNSS 2007). Fort Worth, TX, 866–875.
Wanninger, L., & Beer, S. (2015). BeiDou satellite-induced code pseudorange variations: Diagnosis and therapy. *GPS Solutions, 19*(4), 639–648. https://doi.org/10.1007/s10291-014-0423-3
Wu, J. T., Wu, S. C., Hajj, G. A., et al. (1993). Effects of antenna orientation on GPS carrier phase. *Manuscripta Geodaetica, 18*, 91–98.
Wübbena, G. (1985). Software developments for geodetic positioning with GPS using TI-4100 code and carrier measurements. In: *Proceedings of the first international symposium on precise positioning with the global positioning system*, Rockville, MD, April 5–19.
Yang, Y., Mao, Y., & Sun, B. (2020). Basic performance and future developments of BeiDou global navigation satellite system. *Satellite Navigation, 1*, 1. https://doi.org/10.1186/s43020-019-0006-0
Yang, Y., Song, L., & Xu, T. (2002). Robust estimator for correlated observations based on bifactor equivalent weights. *Journal of Geodesy, 76*(6), 353–358. https://doi.org/10.1007/s00190-002-0256-7
Zhao, L., Ye, S., & Chen, D. (2019). Numerical investigation on the effects of third-frequency observable on the network clock estimation model. *Advances in Space Research, 63*(9), 2930–2937. https://doi.org/10.1016/j.asr.2018.03.004
Zhao, Q., Guo, J., Wang, C., et al. (2022). Precise orbit determination for BDS satellites. *Satellite Navigation, 3*, 2. https://doi.org/10.1186/s43020-021-00062-y
Zhou, W., Cai, H., Chen, G., Jiao, W., He, Q., & Yang, Y. (2022). Multi-GNSS combined orbit and clock solutions at iGMAS. *Sensors, 22*(2), 457. https://doi.org/10.3390/s22020457
Zuo, X., Jiang, X., Li, P., et al. (2021). A square root information filter for multi-GNSS real-time precise clock estimation. *Satellite Navigation, 2*, 28. https://doi.org/10.1186/s43020-021-00060-0

Publisher's note